Proceedings of ASME Turbo Expo 2009: Power for Land, Sea and Air
GT2009
June 8-12, 2009, Orlando, Florida, USA

GT2009-59377

Experimental and Numerical Investigation of Convective Heat Transfer in a Gas Turbine Can Combustor

Sunil Patil, Santosh Abraham, Danesh Tafti and Srinath Ekkad
Mechanical Engineering Department
Virginia Polytechnic Institute and State University
Blacksburg VA 24061 USA
&
Yong Kim, Partha Dutta, Hee-Koo Moon and Ram Srinivasan
Solar Turbines, Incorporated
San Diego, CA

ABSTRACT

Experiments and numerical computations are performed to investigate the convective heat transfer characteristics of a gas turbine can combustor under cold flow conditions in a Reynolds number range between 50,000 and 500,000 with a characteristic swirl number of 0.7. It is observed that the flow field in the combustor is characterized by an expanding swirling flow which impinges on the liner wall close to the inlet of the combustor. The impinging shear layer is responsible for the peak location of heat transfer augmentation. It is observed that as Reynolds number increases from 50,000 to 500,000, the peak heat transfer augmentation ratio (compared to fully-developed pipe flow) reduces from 10.5 to 2.75. This is attributed to the reduction in normalized turbulent kinetic energy in the impinging shear layer which is strongly dependent on the swirl number that remains constant at 0.7 with Reynolds number. Additionally, the peak location does not change with Reynolds number since the flow structure in the combustor is also a function of the swirl number. The size of the corner recirculation zone near the combustor liner remains the same for all Reynolds numbers and hence the location of shear layer impingement and peak augmentation does not change.

NOMENCLATURE

A	Surface area of heater
D	Can combustor diameter
h	Heat transfer coefficient
k	Turbulent kinetic energy
Nu	Nusselt number (hD/ κ)
Pr	Prandtl number
Q	Constant heat flux on liner wall
R	Electrical resistance of heater material
Re	Reynolds number
R_0	Flow injector outer radius
S	Swirl number
U_τ	Friction velocity ($\sqrt{\tau_w / \rho}$)
V	Velocity vector
y^+	dimensionless distance from wall ($\rho U_\tau \eta/\mu$)
x,r,θ	Axial, radial, and azimuthal cylindrical polar coordinates respectively
α	Side wall expansion angle
η	Wall normal distance
ε	Turbulence energy dissipation rate
υ	Electric voltage applied to heater
κ	thermal conductivity
μ	Fluid (air) molecular viscosity
Φ	Swirler vane angle
ρ	Fluid density
τ_w	Wall shear stress

Subscripts

in	Value at inlet to flowfield
c	Based on Can combustor
∞	Free stream flowfield value
0	Reference value
max	Maximum value

INTRODUCTION

Both the desire for better efficiency and the need for lower emissions have reduced the amount of cooling air that the combustion engineer has available for combustor liner cooling. As combustors are designed to reduce emissions, there is insufficient liner cooling available as more air is utilized in the premixing process and reaction zones to maintain as low a temperature as possible. Due to this requirement, the effectiveness of backside cooling techniques involving impingement, convection, or surface enhancement techniques becomes more critical (Chin et al. [1], Metzger et al. [2], Andrews et al[3], Fric et al. [4], Schulz [5], Arellano et al. [6] and Smith and Fahme [7]). Due to longer operating cycles for power turbines, the combustor liner needs to meet durability targets of 30000 hours. To avoid liner failure from over-heating, it is extremely important to accurately quantify the liner heat load accurately in the lean premixed combustor environment. Also, the cooling techniques for the low NO_x combustor liner requires more backside cooling and less or almost no film cooling. The lack of knowledge of the local gas side convective heat transfer distribution on the combustor liner makes effective cooling of liners more difficult. The results from this study will help in understanding and predicting swirling flow effects on the local convective heat load to the combustor liner and thus support the development of more effective cooling schemes to maintain/improve combustor durability. Although radiative load is a significant contributor in the combustor, it is relatively easy to estimate compared to the convective load. In this study, the focus is to understand the convective loading on the liner due to the swirling flow.

Typically, a swirler is used in industrial gas turbines to impart a high degree rotation of flow at the combustor primary zone which helps to promote better air-fuel mixing and to induce a recirculatory flow in the primary zone. During the real lean-burn engine operation, gaseous fuel is injected from a series of fuel nozzles mounted on bluff bodies to premix with main stream intake air. The premixed gaseous fuel-air mixture is then ignited and the flame is stabilized at the recirculation zone behind bluff bodies. Due to the wakes or recirculation vortices, which are caused by turbulent flow boundary layer separation on the surface of the bluff body, the flow transitions to a highly turbulent state so as to provide more energy to the flow and also to help better air-fuel mixing. Furthermore, the recirculation zone behind the bluff body contributes as a flame stabilizer to help trap the flame at high speed flow conditions.

Most of the studies investigating swirling jet structure involved measurement of mean velocities and turbulence quantities. Gore and Ranz [8] characterized the recirculation zone in swirling flows with varying geometric conditions. Reduction in jet centerline velocity was observed indicating existence of an axial pressure gradient. They concluded that the jet spread angle as function of applied swirl. Chigier and Chervinsky [9] also observed jet spread angle to be a function of applied swirl. Brum and Samuelson [10] reported two-component LDV measurements in an axisymmetric combustor model with coaxial swirling jets. Vu and Gouldin [11] reported hot wire measurements in an axisymmetric combustor. In recirculation zones, tangential velocities were found to be very small while levels of turbulence and dissipation rate were very high. Rhode and Lilley [12] performed mean flow-field studies in axisymmetric combustor geometries with swirl. Various flow-field configurations with different side wall angles and swirl vane angles were investigated to characterize the time-mean streamlines, recirculation zone and regions of high turbulence. The length and width of the recirculation zone was found to increase with increase in swirl vane angle until a critical angle was reached, after which any further increase in swirl shortened the length but further increased the width. The major effect of side wall expansion angle was to shorten the corner recirculation region, with no major effect on the central recirculation region. Ferrell, Abujalela, Busnaina and Lilley [13] reported experiments with five-hole pitot probe velocity measurements and flow visualization.

Bailey et al [14] conducted experimental and numerical simulations to characterize heat transfer on F class combustor liner cooled by impingement jets and cross flow between liner and sleeve. Calculations were performed using various RANS based turbulence models with different near wall treatments. Of particular interest is that a two layer model approach gave better predictions compared to wall functions. Thundil and Ganeshan [15] studied the effect of various geometric parameters like vane angle, vane number, hub to tip ratio on flow development downstream of the swirler. They characterized swirl flow by the size of the recirculation zone, mass trapped in it and axial pressure drop. Fernando et al [16], Grinstein and Fureby [17] reported LES studies of flow in swirl combustors.

The objective of the present study is to use experiments and computations to investigate the effect of Reynolds number on liner wall convective heat transfer coefficient in a can combustor. An engine scale swirler is used to simulate the actual flow conditions downstream of the swirler. The numerical calculations investigated RANS (Reynolds Averaged Navier Stokes) based turbulence models to predict the swirling flow and surface heat transfer coefficients. For comparison, different turbulence models, such as, standard, realizable and RNG (Re-Normalization Group theory) k-ε, SST (Shear Stress Transport) were tested. It is shown that for a given swirl number, the location of peak heat transfer augmentation is quite independent of the Reynolds number, whereas the augmentation ratio decays considerably as the Reynolds number increases. The study is unique in that these trends on combustor liner gas side wall heat transfer have never been captured and explained in the literature and have important implications on the design of liner wall cooling systems.

EXPERIMENTAL INVESTIGATION

Figure 1 shows a schematic of the experimental set up used to measure heat transfer coefficients on combustor liner wall. The air supply was provided by a pressure blower whose motor was controlled by an adjustable frequency drive to obtain the required flow rate. This flowrate, measured by pitot probe, was adjusted to obtain the required Reynolds number. The air was passed into the combustor chamber through the swirler fitted at its entry. An Infrared (IR) camera was used to measure the surface

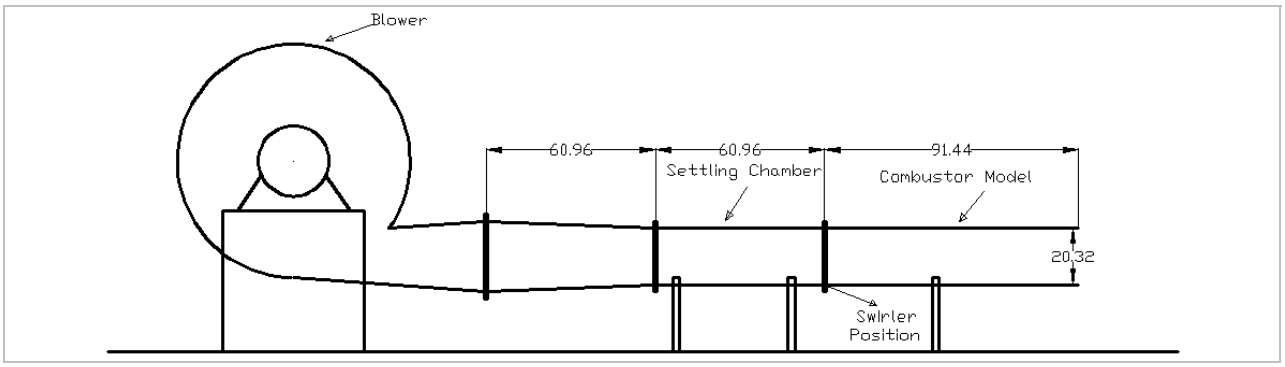

Figure 1 Experimental Setup (all dimensions are in cm)

temperature on the combustor liner wall, which was heated using two resistance surface heaters to provide a uniform wall heat flux boundary condition. From the blower, the air flows into the a 203-mm circular duct which serves also as a flow stabilization chamber before it is passed through a typical combustor nozzle with a 20-vane axial flow swirler retrofitted at the end of the duct. The flow then enters the combustor can simulator which is a 203-mm circular duct with surface heaters on one sector of the diameter and windows on the opposite side of the heated wall to allow the IR camera to monitor wall temperatures. Thermocouples were placed upstream of the swirler to obtain the inlet temperature and on the surface of the heater foil to calibrate the IR camera. A pitot probe was positioned in the flow stabilization chamber to obtain accurate value of the mean velocity of air in the can combustor.

Figure 2 shows the model of the swirler that was used in this study. The swirler has an outer diameter of 79.25-mm and an inner diameter of 44.45-mm. The flow enters the annulus from the 200-mm duct upstream and squeezes into the annulus before being turned by the 20-vanes through an angle of 45^{o}. The rods just downstream of the vanes are fuel injectors that are inactive in this study.

The combustion simulator section was fabricated using acrylic material to simulate a low conductivity material to allow for minimal heat loss from the back of the heater. As indicated earlier, windows for positioning the IR camera lens were cut with equal spacing at six different locations along the main combustion chamber for heat transfer experiments, shown in Figure 3. Diametrically opposite side to these windows, a surface heater assembly was mounted along the combustor wall. The entire combustor simulator was then covered with insulating material to minimize heat loss. At any time, the test surface was viewed through one of the windows. The other windows were used for different axial locations along the liner wall. Each of the unused IR camera window holes was sealed during tests. A pitot probe was inserted into the chamber to ascertain the air velocity values. In order to obtain constant heat flux boundary conditions at the liner wall, the combustor wall diametrically opposite the IR windows was fitted with 2 surface heaters commercially obtained from Minco (www.minco.com) that extend 32 inches length from the combustor inlet along the axial direction and covered 60-deg of the circumference of the can combustor duct. The temperature on the heater was measured to be constant with no flow for a certain known heat flux to ensure a constant heat flux surface.

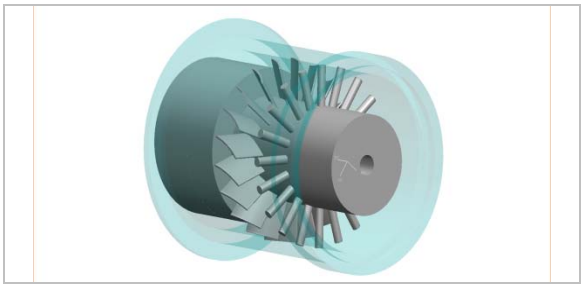

Figure 2 3D CAD model of Swirler

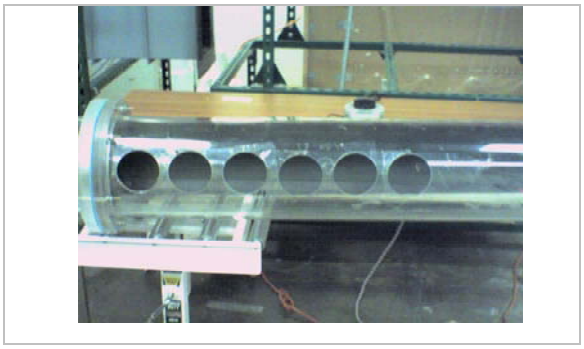

Figure 3 Viewports for IR camera on combustor model wall

Figure 4 shows the schematic of the surface heater system construction for the steady-state experiment. The face of the heater exposed to the IR camera inside the combustor was coated with thin flat black paint for increase surface emissivity. The other face was glued on to the acrylic combustor wall. Heat input from the heater was adjusted using transformers by varying the voltage and amperage to obtain the required power output.

A FLIR SC640 Infrared Camera was used to capture the liner wall surface temperature distribution along the combustor liner wall. The SC640 camera is a focal plane array system type IR camera using microbolometer as detector material and has thermal sensitivity as high as within 0.1ºC at 30ºC. The camera has a maximum resolution of 640x480 and wide measurement range of -40°C to +1,500°C, in 3 ranges. With proper calibration temperatures up to + 2000°C can be recorded. The target surface emissivity can be precisely calibrated with its full emissivity adjustment from 0.1 to 1.00. The refresh frequency of imaging can be set as high as 60Hz.

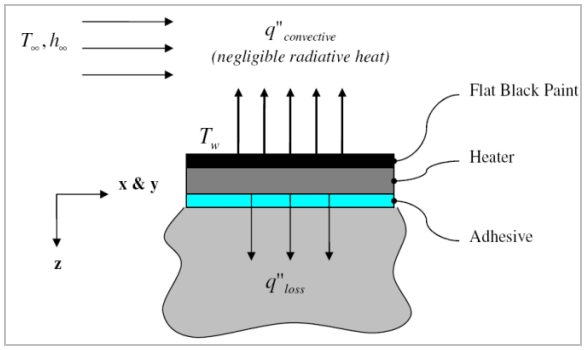

Figure 4 Schematic of surface heater

HEAT TRANSFER MEASUREMENT METHODOLOGY

Air at room temperature from the blower was sent into the main combustion simulator duct through the swirler mounted concentrically within the inlet chamber. The heat flux was adjusted using two variable transformers to obtain the desired temperature difference between the wall and the bulk air. The inlet upstream and exit downstream air temperatures were measured with high sensitivity fine gage K-type thermocouples using the OMB-DAQ-54 Personal Daq USB Data Acquisition Module temperature measuring system. Surface mounted thermocouples on the heater foil were also used to calibrate the IR camera to ensure accurate measurements. The entire set up was left running for at least an hour until a steady-state wall surface temperature is reached. The entire combustor simulator duct was covered with insulating material to prevent heat losses. The experimental heat loss (Q_{loss}) was determined by running the heaters at the test operating temperature and measuring the heat flux without flow. Typically, the heat loss was obtained to be less than 5% of the heat input to through the heaters. The IR image of temperature distribution was acquired at six different locations along the combustion chamber. The raw temperature data from all six different images were merged and combined to compute the local heat transfer coefficient distributions. The basic convective heat transfer equation was used.

$$h = \frac{Q - Q_{loss}}{A(T_{wall} - T_{air})} \qquad (1)$$

The heat input was calculated using the resistance ratings of the heater and the voltage settings on the transformer. Typical heat flux input values were 1500 W/m^2 and the wall temperatures during the experiment were between 30-60^{o}C.

$$Q = \frac{\upsilon^2}{R} \qquad (2)$$

The target surface emissivity for the IR measurement was calibrated using an OMEGA cement-on thermocouple and the OMB-DAQ-54 Personal Daq Data Acquisition system temperature measuring system and was determined to be 0.92. Overall uncertainty in heat transfer coefficient was estimated to be around ±6.4% using the methodology of Kline and McClintock [21]. Uncertainty in flow Reynolds number was estimated to be ±4%.

COMPUTATIONAL METHODOLOGY

A full three dimensional incompressible steady state analysis was carried out using the commercial software FLUENT [18] to characterize heat transfer on the liner wall as well as to visualize and understand the effect of strong swirl. Figure 5 shows the computation domain consisting of a periodic segment of the injector and the can combustor. The flow in a single passage of the injector swirler vanes is simulated. It consists of an annular inlet section, followed by the swirler vanes, the fuel injector followed by a straight section of the injector which opens into the can combustor. The computational domain was mapped using a multi-block structured mesh with total 3.4 million hexahedral cells. Figure 6 shows the boundary layer resolution near the swirler vanes and combustor liner walls.

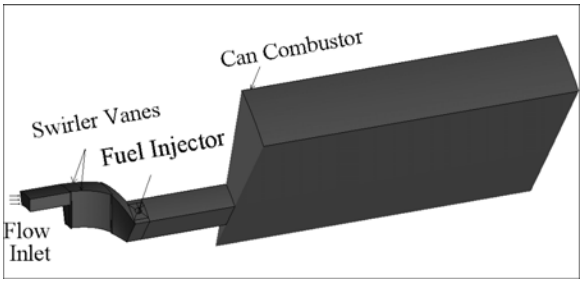

(a)

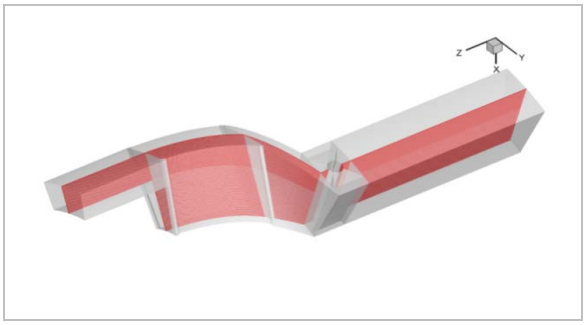

(b)

Figure 5 (a)Computational Domain (b) overall mesh view in flow nozzle (sector angle = 18)

For the RANS calculations, two approaches were used to resolve the boundary layer. For low Reynolds flows (Re = 50,000 and Re = 80,000), wall integration was used as the near wall treatment with y^+ values in the range of 1 to 5. The wall function approach was more economical at high Reynolds numbers with y^+ ranging from 30 to 100.

Table 1 summarizes the numerical calculations and Table 2 summarizes the boundary conditions used in the numerical investigation. The inlet section of the computational domain was given a boundary condition of mass flow inlet based on Reynolds number. Reynolds number was increased using higher inlet velocity (for 50,000 and 80,000 case) and higher density(for Re=300,000 and above). Periodic boundary conditions were specified in the azimuthal direction, and an outflow condition was used at the combustor exit. The rest of the domain surfaces including vanes were assigned wall (no slip) boundary conditions. A surface heat flux value was specified for the combustor liner wall while all other walls were treated as adiabatic.

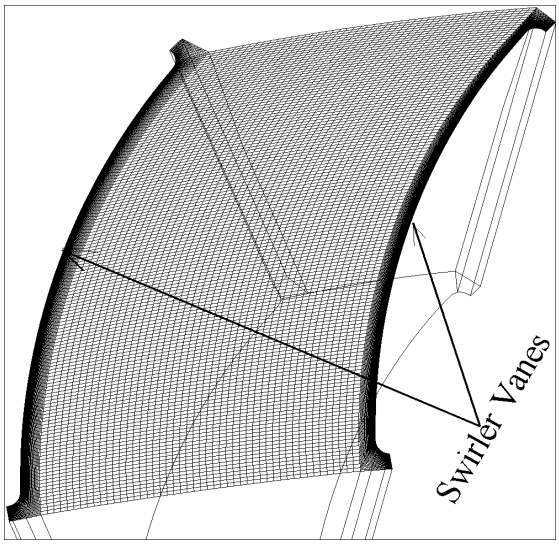

(a)

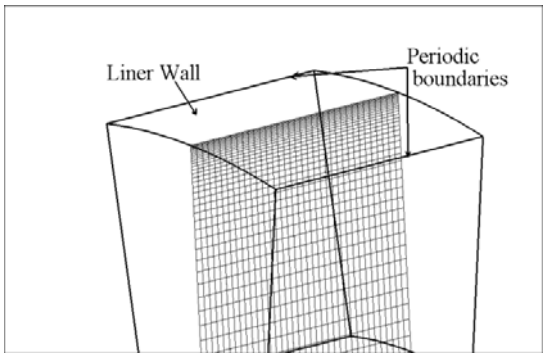

(b)

Figure 6 (a) Boundary layer resolution near swirler vane and (b) Near liner wall

Table 1 Numerical calculation summary

Reynolds number	Turbulence model	Near wall treatment	Mesh adaptivity
50,000	Standard k-ϵ Realizable k-ϵ RNG k-ϵ SST k-ω RSM	Wall integration	Applied based on y^+
80,000	RNG k-ϵ	Wall integration	Applied based on y^+
300,000	RNG k-ϵ	Wall function	Not applied
350,000	RNG k-ϵ	Wall function	Not applied
400,000	RNG k-ϵ	Wall function	Applied based on y^+
500,000	RNG k-ϵ	Wall function	Applied based on y^+

Table 2 Boundary conditions

Computational face	**Flow BC**	**Thermal BC**
Inlet	Mass inflow / Velocity Inlet	(Ref. Temp = 294K)
Outlet	Outflow	-
External Periodic	Periodic	Periodic
Liner wall	No slip	Surface heat flux specified
Hub, casing, vanes and injector pins	No slip	Adiabatic (surface heat flux= 0)

RESULTS

EXPERIMENTAL HEAT TRANSFER COEFFICIENT DISTRIBUTION

Figure 7 presents the detailed heat transfer coefficient distributions on the liner wall as obtained from the measurements in the experimental set-up. Six different window images are used to generate a comprehensive heat transfer profile in the axial direction. Results for two flow Reynolds numbers are presented from the start of the canned combustor at the exit of the swirler to the combustor exit. The slight mismatches in heat transfer coefficient at frame boundaries are within experimental uncertainty. The heat transfer coefficient is low at the immediate entrance to the canned combustor but quickly reaches a maximum value after which the magnitude decays slowly. It is shown later that the heat transfer

distribution largely correlates with the hydrodynamics of the strongly swirling flow that issues from the injector.

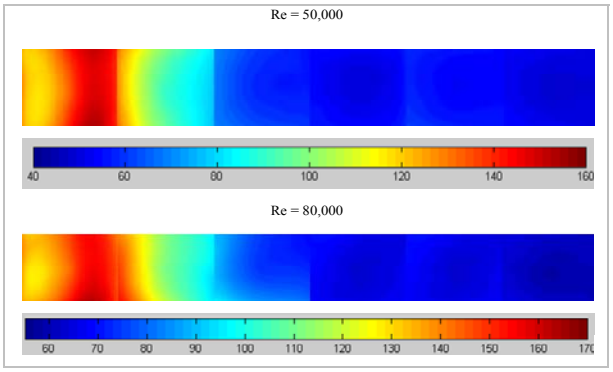

Figure 7 Detailed heat transfer distributions on the liner wall (left: swirler; right: exit)

VALIDATION OF COMPUTATIONAL MODEL

A number of different turbulence models were tested for their ability to predict the strongly swirling flow in the combustor. Figure 8 compares results of various turbulence models used in the calculations with experimental data for a Reynolds number of 50,000. The heat transfer coefficient at the liner wall is characterized by the Nusselt number augmentation ratio, where the baseline Nusselt number is obtained from the Dittus-Boelter correlation for fully-developed flow

$$Nu_0 = 0.023\,\mathrm{Re}^{0.8}\,\mathrm{Pr}^{0.3} \qquad (3)$$

The results are plotted versus axial distance normalized by the can duct diameter. It was found that RNG model with swirl modification and differential viscosity model [18] predicted the results in best agreement with experiments. The model predicted both the location and magnitude of peak heat transfer in exact agreement with experiments. However, some difference between the model prediction and experiments exist downstream of the peak location. It was found that the SST model over predicted the values of peak heat transfer coefficients while the standard and realizable k-ε models under predicted it. Also the peak location is predicted downstream of the experimental measurements. It is clear from this comparison that the RNG model predicts the highly strained swirl flow coming out of the injector with much better fidelity than the other models. Hence, the RNG model is used for investigating the effect of Reynolds number on heat transfer.

Figure 9 further compares predictions with experiments at Re=50,000 and 80,000 using the RNG k-ε model. It is observed that the predictions compare very well with experiments at Re=80000. More importantly, it is also observed that the location of peak heat transfer remains the same but the magnitude of peak augmentation reduces from approximately 10 to 8. This is explained by investigating the flow field in the combustor in more detail.

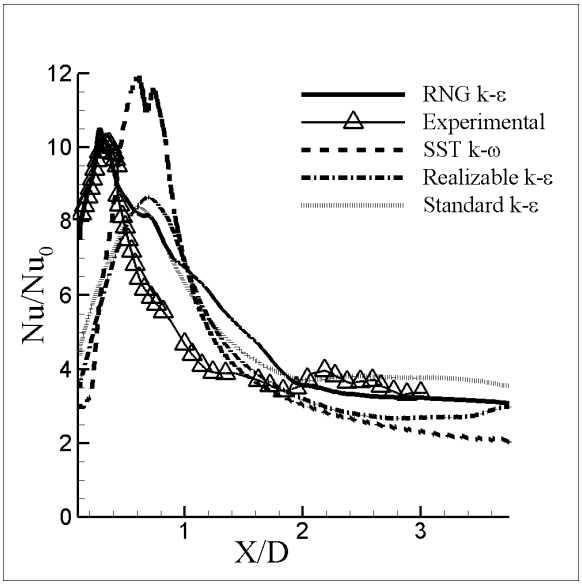

Figure 8 Comparison of numerical predictions using different turbulence models with experiments at Re=50,000

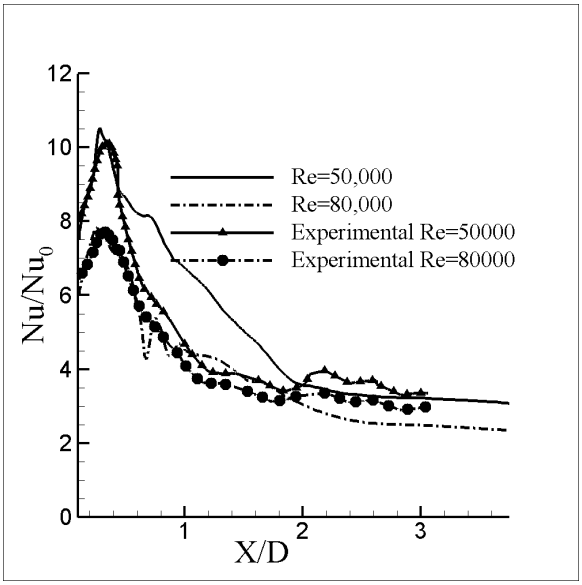

Figure 9 Nusselt number augmentation for Re=50,000 and Re= 80,000 along the liner wall

FLOW FIELD CHARACTERISTICS

Figures 10 through 12 characterize the flowfield for a Reynolds number of 50,000. The streamline plot in Figure 12 expresses two main features of swirl flow in the combustor geometry, a corner recirculation zone and a central recirculation zone. The presence of the central recirculation zone indicates that the swirl number is beyond

the critical value of 0.6. The swirl number is defined as the ratio of tangential momentum to axial momentum and is calculated as

$$S = \frac{\int r V_\theta V_x dr}{R_0 \int r V_x^2 dr} \quad (4)$$

at an axial plane near the injector exit to be 0.7. The computational flow structure is in complete agreement with past studies [12].

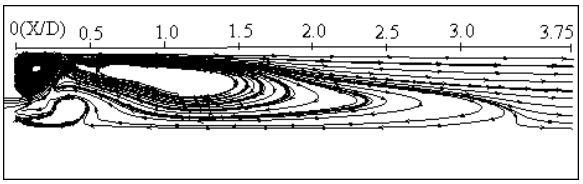

Figure 10 Streamlines in combustor (Re = 50,000)

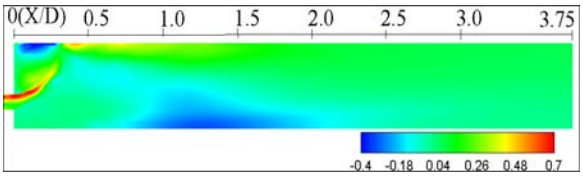

Figure 11 Contours of normalized axial velocity in meridional plane in combustor (Re = 50,000)

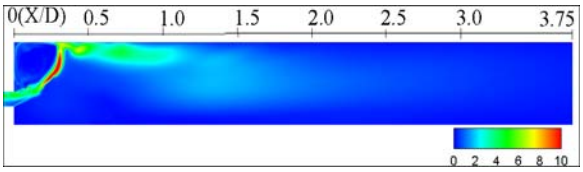

Figure 12 Contours of normalized turbulent kinetic energy in meridional plane in combustor (Re = 50,000)

Figures 10, 11, and 12 show that the location of the peak heat transfer coincides with the impingement of the highly energetic shear layer issuing from the injector. The flow impingement can be visualized with contours of normalized axial velocity and turbulent kinetic energy. A large augmentation in heat transfer coefficient is observed because of the very high values of axial velocity and turbulent kinetic energy near the impingement location. Furthermore, the spread angle of flow expanding into the can combustor is much higher than that without swirl, which results in flow impingement very close to the inlet of the combustor (X/D=0.3) with higher axial velocity. This is the main mechanism responsible for the location and peak magnitude of heat transfer augmentation.

Figure 13 shows the distribution of axial velocity along the radial direction at various axial locations in the combustor. The radial traverses were obtained at a location on axial plane, midway between the two blades. Note that r/D = 0.2 is the radial location of the outer casing of the flow injector in which the swirler vanes are attached. The axial velocity is normalized with the flow inlet velocity U_{in}. At the combustor inlet, the axial velocity varies from zero at the hub of the swirler vane position to a maximum near the injector casing in a near linear distribution. The axial velocity shows a step at r/D = 0.12 because of the presence of the recirculation zone. Similar trends were noted by Lilley [20]. As we move away from the combustor inlet, the location of peak axial velocity moves radially outward. Figure 13 also compares these radial traverses at X/D = 0 and X/D = 0.5 with experimental data of Rhode and Lilley [12] with a similar geometry (vane angle = 45^0 and side wall expansion angle of 90^0). Very close agreement is observed with the measurements.

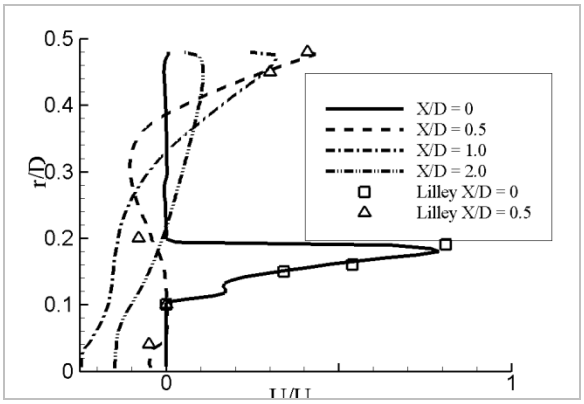

Figure 13 Normalized axial velocity profiles for radial traverse

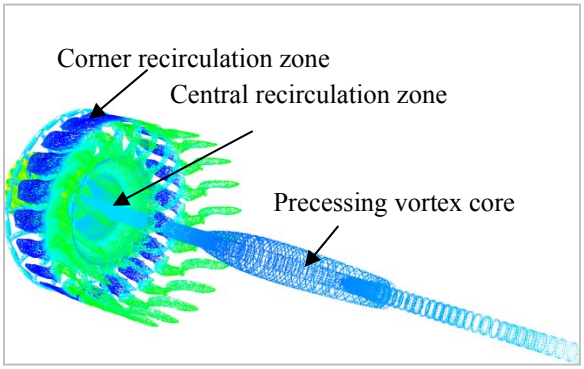

Figure 14 Axial vorticity isocontour (value = 1000) in combustor colored with axial velocity.

Figure 14 visualizes the 3D swirl dominated flowfield by replicating the computation domain in the azimuthal direction to cover the full combustor. The isocontours (value = 1000) of vorticity colored with axial velocity are shown. Structures of corner recirculation zone, central recirculation zone and precessing vortex core show good qualitative agreement to the experimental visualization provided by Rhode and Lilley [12] for a similar geometry.

EFFECT OF REYNOLDS NUMBER

Figure 15 shows the effect of Reynolds numbers ranging from 50,000 – 500,000 on the location and

magnitude of the computed heat transfer coefficient along the combustor liner wall. It is clear that the peak value of heat transfer augmentation factor reduces with an increase in Reynolds number but the location of the peak value does not change with increasing Reynolds number.

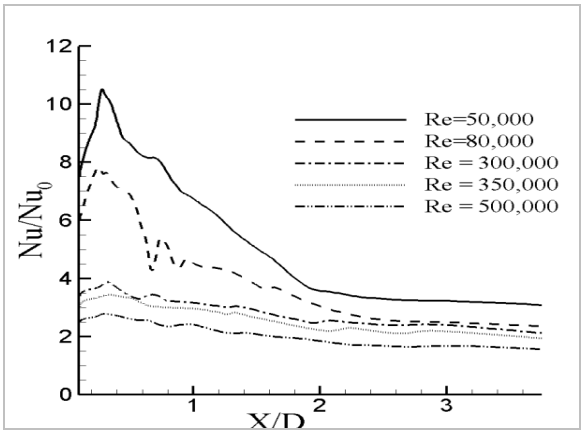

Figure 15 Effect of Reynolds number on liner wall heat transfer augmentation.

Figure 16 shows the variation of peak Nusselt number augmentation with Reynolds number. The numerical values match in very close agreement with experimental results at 50,000, 80,000 and 500,000. Experimental data for 500,000 was reported by Goh [19] on exactly the same geometry on an experimental set up with a scaling factor of 5.

The large drop in augmentation ratio but the invariability of the location of peak heat transfer with Reynolds number is explained in the following manner.

Figure 17 shows the variation of turbulent kinetic energy (TKE) normalized with the square of mean velocity in the can combustor at a location near the peak heat transfer. Since in most shear flows, wall heat transfer is largely dependent on the magnitude of near wall turbulent quantities, the T.K.E magnitude close to the wall is a good indicator of turbulent activity. The plot shows that the normalized T.K.E. reduces with Reynolds number, hence explaining why the heat transfer coefficient augmentation ratio decreases with an increase in Reynolds number (it is noted that the heat transfer coefficient increases with Reynolds number). The T.K.E. production in the impinging shear layer is dependent on the Reynolds number as well as the degree of swirl. However, it is noted that even with the increase in Reynolds number the swirl number remains constant at 0.7 since it is largely dependent on the injector vane geometry. Hence, although turbulent production increases in the impinging shear layer as a result of increased Reynolds number, the normalized value decreases because it is strongly dependent on the swirl number which remains the same.

The relative invariability of the peak location with Reynolds number can also be explained by the constant swirl number. The primary reason for this is that the flow pattern established in the combustor is independent of the Reynolds number. Figure 18 shows the streamline structure in the combustor for Reynolds numbers of 80,000 and 500,000. It is seen that the overall flow structure changes very little and hence the location of impingement remains fairly constant over the range of Reynolds numbers.

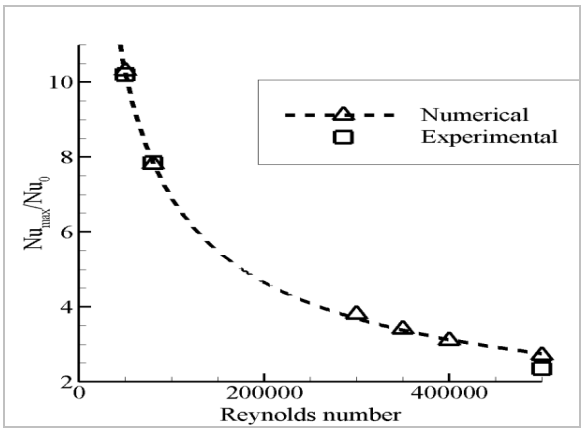

Figure 16 Variation of peak heat transfer augmentation ratio with Reynolds number

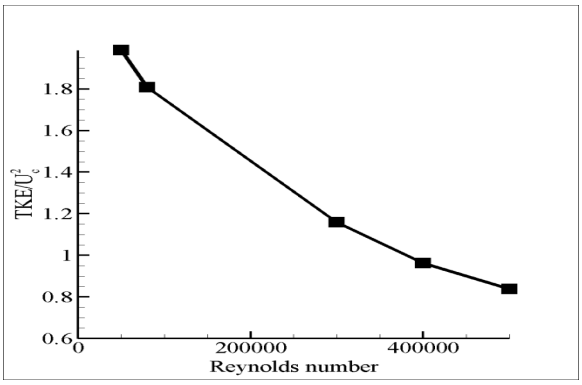

Figure 17 Variation of normalized turbulent kinetic energy with Reynolds number near shear layer impingement on liner wall

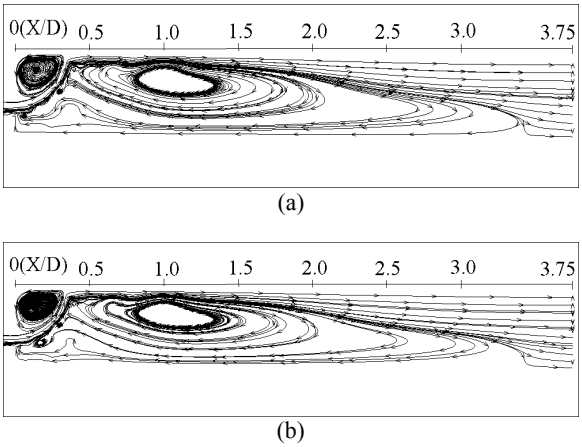

(a)

(b)

Figure 18 Streamlines in combustor for (a) Re = 80,000 and (b) Re = 500,000 .

SUMMARY AND CONCLUSIONS

Experiments and numerical computations were performed to investigate the heat transfer characteristics of a gas turbine can combustor under cold flow conditions. An engine scale can combustor and swirler nozzle were used in the experiment. The walls of the combustor were instrumented with a surface heater to produce a constant surface heat flux. Cold mainstream air was used in the combustor for the steady state heat transfer test. The surface temperature was measured using an infra-red camera, and local heat transfer coefficients were computed from the known wall heat flux, mainstream air temperature and the measured wall temperature.

The numerical calculations investigated RANS based turbulence models to predict the swirling flow and surface heat transfer coefficients. The RNG turbulence model was best suited for the swirl dominated flow. Results for peak heat transfer augmentation factor and location were in close agreement with experimental predictions.

It is observed that the flow field in the combustor is characterized by an expanding swirling flow which impinges on the liner wall close to the inlet of the combustor. The impinging shear layer is responsible for the peak location of heat transfer augmentation. It is observed that as Reynolds number increases, the peak heat transfer augmentation ratio reduces, while the peak location remains the same. This is attributed to the reduction in normalized turbulent kinetic energy in the impinging shear layer which is strongly dependent on the swirl number that remains constant at 0.7 with Reynolds number. Additionally, since the flow structure in the combustor is also a function of the swirl number, it does not change with Reynolds number. The size of the corner recirculation zone near the combustor liner remains the same for all Reynolds numbers and hence the location of shear layer impingement and peak augmentation does not change.

ACKNOWLEDGEMENT

The primary authors would like to acknowledge the support provided by Solar Turbines, Incorporated for funding this work.

REFERENCES

[1] Chin, J., Skirvin, S., Hayes, L., and Burggraf, F., 1961, "Film Cooling with Multiple Slots and Louvers – Part 1: Multiple Continuous Slots", *Journal of Heat Transfer*, Vol. 83, pp. 281-286.

[2] Metzger, D.E., Takeuchi, D., and Kuenstler, P., 1973, "Effectiveness and Heat Transfer with Full-Coverage Film Cooling", *Journal of Engineering for Power*, Vol. 95, pp. 180-184.

[3] Andrews, G.E., Khalifa, I.M., Asere, A.A., Bazdidi-Tehrani, F., 1995, "Full Coverage Effusion Film Cooling with Inclined Holes", Paper 95-GT-274, IGTI Turbo Expo, Houston.

[4] Fric, T.F., Campbell, R.P., and Rettig, M.G., 1997, "Quantitative Visualization of Full-Coverage Discrete-Hole Film Cooling", Paper 97-GT-328, IGTI Turbo Expo, Orlando.

[5] Schulz, A., 2001, "Combustor Liner Cooling Technology in Scope of Reduced Pollutant formation and Rising Thermal Efficiencies", in *Heat Transfer in Gas Turbine Systems*, Annals of the New York Academy of Sciences, Vol. 934, pp. 135-146.

[6] Arellano, L., Smith, K., and Fahme, A., "Combined Back Side Cooled Combustor Liner and Variable Geometry Injector Technology", ASME Paper 2001-GT-0086, 2001

[7] Smith, K. and Fahme, A., 1999, "Backside Cooled Combustor Liner for Lean-Premixed Combustion", Paper No. 99-GT-239, IGTI Turbo Expo, Indianapolis.

[8] Gore, R.W., Ranz, W.E., "Backflow in Rotating Fluids Moving Axially through Expanding cross Sections", A.I.Ch.E. Journal. Vol. 10, January, 1964, pp. 83-88.

[9] Chigier, N.A., Chervinsky, A, "Experimental Investigation of Swirling Vortex Motion in Jets" Transactions of ASME, Journal of Applied Mechanics, June, 1967, pp 443-450.

[10] Brum, R.D., Samuelson, G.S., "Two-Component Laser Anemometry Measurements of Non-reacting and Reacting Complex flows in a swirl-stabilized model combustor", Experiments in Fluids, Vol. 5, 1987, pp. 95-102.

[11] Vu, B.T., Gouldin, F.C., "Flow Measurement in a Model Swirl Combustor", AIAA Journal, Vol. 20, May, 1982, pp. 642-651.

[12] Rhode, D.L., Lilley, D.G., McLaughlin, D.K., "Mean Flowfields in Axisymmetric Combustor Geometries with Swirl", AIAA Journal, Vol. 21, April, 1983, pp. 593-600.

[13] Ferrell, G.B., Abujelala, M.T., Busnaina, A.A., Lilley, D.G., "Lateral Jet Injection into Typical Combustor Flowfields", AIAA Paper No. 84-0374, Presented at the AIAA 22nd Aerospace Sciences Meeting, Reno, Nevasa, January, 1984.

[14] Bailey, J.C., Intile, J., Fric, T.F., Tolpadi, A.K., Nirmalan, N.V., Bunker, R.S., 2003, "Experimental and Numerical Study of Heat Transfer in a Gas Turbine Combustor Liner", ASME J. Eng. For gas turbines and power, Vol. 125, pp. 994-1002.

[15] Raj, T.K.R., Ganeshan V., 2008, "Study on the Effect of various Parameters on Flow development behind Vane Swirlers", Int. J. Thermal Sciences, Vol. 47, pp. 1204-1225.

[16] Fernando, F., Grinstein, T., Young, R., Gutmark, E. J., Li, G., Hsiao, G., Mongia, H.C., 2002, "Flow Dynamics in a Swirl Combustor", J. Turb. 3, Vol. 3

[17] Grinstein, F., Fureby, C., 2005, "LES Studies of the Flow in a swirl gas combustor", Proc. Combustion Institute, Vol 30, pp. 1791-1798.

[18] FLUENT 6.3 User's Guide. Fluent Inc., 2007.

[19] Goh, Y., "Heat Transfer and Flow Characteristics inside a gas turbine combustor", MS Thesis, Department of Mechanical Engineering, Louisiana State University, 2006.

[20] Lilley, D. G., 1999, "Annular Vane Swirler Performance", Journal of Propulsion and Power, Vol.15

[21] Kline SJ, McClintock FA, 1953, "Describing uncertainties in single sample experiments," Mechanical Engineering, Vol. 75, pp. 3–8.